Hydraulic Efficiency of Green-Blue Flood Control Scenarios for Vegetated Rivers: 1D and 2D Unsteady Simulations

Giuseppe Francesco Cesare Lama [1,2,*], Matteo Rillo Migliorini Giovannini [3], Alessandro Errico [3], Sajjad Mirzaei [4], Roberta Padulano [5], Giovanni Battista Chirico [1] and Federico Preti [3]

1. Department of Agricultural Sciences, Water Resources Management and Biosystems Engineering Division, University of Naples Federico II, 80055 Portici, Italy; giovannibattista.chirico@unina.it
2. Department of Civil, Architectural and Environmental Engineering (DICEA), University of Naples Federico II, 80125 Napoli, Italy
3. Department of Agricultural, Food, Environmental and Forestry Sciences and Technologies, University of Florence, 50144 Firenze, Italy; matteo.rillomigliorinigiovannini@unifi.it (M.R.M.G.); alessandro.errico@unifi.it (A.E.); federico.preti@unifi.it (F.P.)
4. Faculty of Natural Resources and Marine Sciences, Tarbiat Modares University, 14115-111 Noor, Iran; Sajjadmirzaei@modares.ac.ir
5. Impacts on Agriculture, Forests and Ecosystem Services (IAFES) Division, Fondazione Centro Euro-Mediterraneo sui Cambiamenti Climatici, 01100 Viterbo, Italy; roberta.padulano@cmcc.it
* Correspondence: giuseppefrancescocesare.lama@unina.it; Tel.: +39-081-253-9423

Abstract: Flood hazard mitigation in urban areas crossed by vegetated flows can be achieved through two distinct approaches, based on structural and eco-friendly solutions, referred to as grey and green–blue engineering scenarios, respectively; this one is often based on best management practices (BMP) and low-impact developments (LID). In this study, the hydraulic efficiency of two green–blue scenarios in reducing flood hazards of an urban area crossed by a vegetated river located in Central Tuscany (Italy), named Morra Creek, were evaluated for a return period of 200 years, by analyzing the flooding outcomes of 1D and 2D unsteady hydraulic simulations. In the first scenario, the impact of a diffuse effect of flood peak reduction along Morra Creek was assessed by considering an overall real-scale growth of common reed beds. In the second scenario, riverine vegetation along Morra Creek was preserved, while flood hazard was mitigated using a single vegetated flood control area. This study demonstrates well the benefits of employing green–blue solutions for reducing flood hazards in vegetated rivers intersecting agro-forestry and urban areas while preserving their riverine ecosystems. It emerged that the first scenario is a valuable alternative to the more impacting second scenario, given the presence of flood control areas.

Keywords: ecohydraulics; BMP; flood control; urban areas; vegetated flows; unsteady hydraulic simulations; LID; green–blue scenarios

1. Introduction

The geo-hydrological and ecohydraulic challenges linked to current and future climate processes [1–6] highlight the growing need to protect water resources quantitatively and qualitatively in an ever more decisive way, especially in sensitive areas within both natural and urban territories [7,8]. In this context, the hydraulic conveyance of vegetated open channels intersecting anthropogenic settlements is dramatically affected by the temporal evolution of riverine vegetation properties [9–11], mainly associated with riverine plants' growth, foliage, and density overall [12,13]. In fact, in the case of vegetated flows, the morphometric and bio-physical changes over time in riverine vegetation canopy features represent a source of hydraulic roughness, in addition to that due to the only riverbanks and bed, to be meticulously considered in the field-scale analysis of global flow resistance [14,15].

Managing riverine vegetation biomass growth plays a key role in mitigating the flooding risk associated with urban and agro-forestry areas crossed by vegetated water bodies [16–19]. In the past, flood peak control has been essentially achieved by adopting hydraulic engineering solutions based on so-called "grey engineering scenarios", aiming at reducing peak hydrological discharge and water levels [20,21] through traditional engineering infrastructures that prevent any development of terrestrial or aquatic ecosystems through the years [22,23]. Thus, grey scenarios do not deliver multiple environmental benefits, also known as "Ecosystem Services", apart from flood control or peak discharge and water level reduction effects. On the other hand, based on the proposal of low-impact developments (LID) and best management practices (BMP), which aim at balancing the need for improved hydraulic efficiency and the need to mitigate the environmental impact of the hydraulic infrastructures, green–blue scenarios constitute a very promising scientific and practical advance in terms of flood control engineering solutions at low ecological impacts [24–29].

To properly model and simulate the actual biomechanical and botanical traits of riverine vegetation stands at field scale, the analysis of the green volumes involved in their phenological and morphometric evolution over time is essential [30–32]. As suggested by previous ecohydraulic studies and reviews [33–35], riverine vegetation's canopy morphometric trends can be easily described by the well-known leaf area index (LAI). This parameter must be properly considered in predictive and numerical modeling of vegetated rivers in urban areas for taking rigorously into account the real-scale impacts of riverine vegetation evolution on flow resistance in vegetated streams, to be then robustly validated by vegetational and water flow measurements acquired during experimental ecohydraulic field campaigns [36,37].

There still exists a need for the proposal of an accurate analytical methodology for evaluating the role of riverine vegetation canopy growth on the effectiveness of green–blue flood risk mitigation systems. To respond to this research question, dedicated hydraulic simulations were carried out in this article to demonstrate the peak flood lamination associated with both riverine vegetation (1D) and natural vegetated flood control areas (2D), as practical examples of green–blue flood control solutions. In detail, the aim of this study is the evaluation of the hydraulic performance (expressed in percentage, %) of two green–blue flood control scenarios associated with peak water level and discharge values for a return period (hereinafter referred to as T) of 200 years in an Italian vegetated river named Morra Creek, colonized by riverine *Phragmites australis* (Cav.) Trin. Ex. Steudel., mostly known as common reed beds. In the first scenario, hereinafter indicated as green–blue Scenario I, the effect of riverine canopy growth on the hydraulic conveyance of the examined vegetated river was simulated by varying the values of Manning's hydraulic roughness coefficients (hereinafter indicated as n) from 0.05 $m^{-1/3}$ s (very young plants) to 0.40 $m^{-1/3}$ s (mature plants) continuously. In the second case, hereinafter referred to as green–blue scenario II, the impacts of the vegetated flood control areas were modeled and simulated, while assuming the cover of the examined riverine vegetation stands along Morra Creek unchanged.

The novel approach proposed in this study is embodied by the analysis of the hydraulic efficiency associated with green–blue flood control proposals, based on the hydrodynamic interaction between the specific riverine vegetation and water flow within a real vegetated watercourse, representing an advance in flood risk mitigation planning applied mainly to vegetated flows crossing agro-forestry and urban areas.

2. Materials and Methods

2.1. Study Site

Morra Basin mainly develops in the two Municipalities of Collesalvetti and Torretta Vecchia (Province of Livorno—Central Tuscany, Northern Italy), from 457 to 18 m a.m.s.l. The land use is mainly constituted by agricultural land, croplands in detail, with about 50% of its surface used for this purpose, while forest and semi-natural environments occupy

43%. The manmade territories cover only 7% but have more than tripled in the last 70 years, affecting mostly floodplains located in the lower part of the Morra Basin watershed. Thus, it is a matter of fact that all this uncontrolled urbanization process contributed importantly to modify the natural hydraulic and ecological conditions of the vegetated stream examined in the present study, which has been progressively forced into increasingly smaller or even channeled both bed and riverbanks through the years.

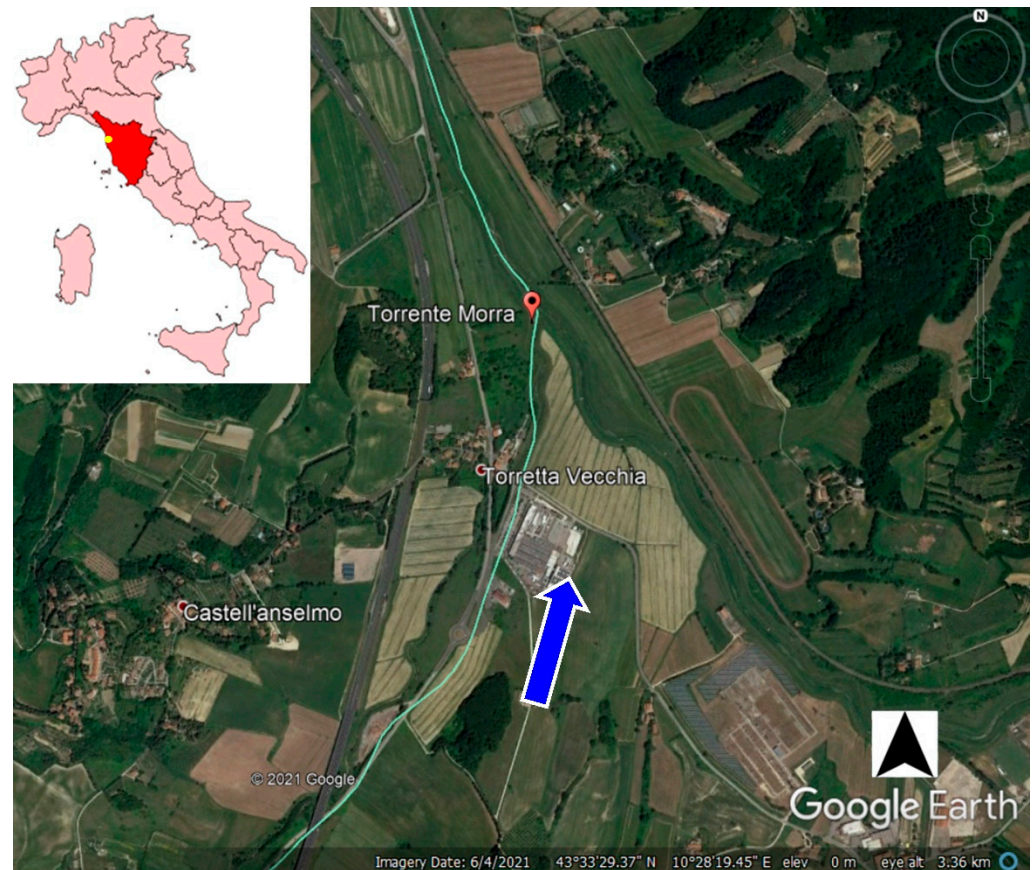Figure 1 shows in detail the Morra Creek's length and location.

Figure 1. Study area (Central Tuscany, Northern Italy) overview. The soft green line indicates Morra Creek, while the blue arrow indicates the flow direction.

Morra Creek (43°33′41″ N–10°28′47″ E, at the vegetated stream's mouth) is a vegetated river belonging to the hydrographic network of Morra Basin. This vegetated watercourse extends for approximately 7 km and the dominant riverine vegetation stands species identified along its length is *Phragmites australis* (Cav.) Trin. Ex. Steudel., commonly known as common reed beds.

In Figure 2, two hydraulic cross-sections of Morra Creek vegetated river are depicted, characterized by the existence of two bridges hereinafter referred to as "Bridge A" (reinforced concrete road bridge) and "Bridge B" (masonry road and pedestrian bridge), respectively.
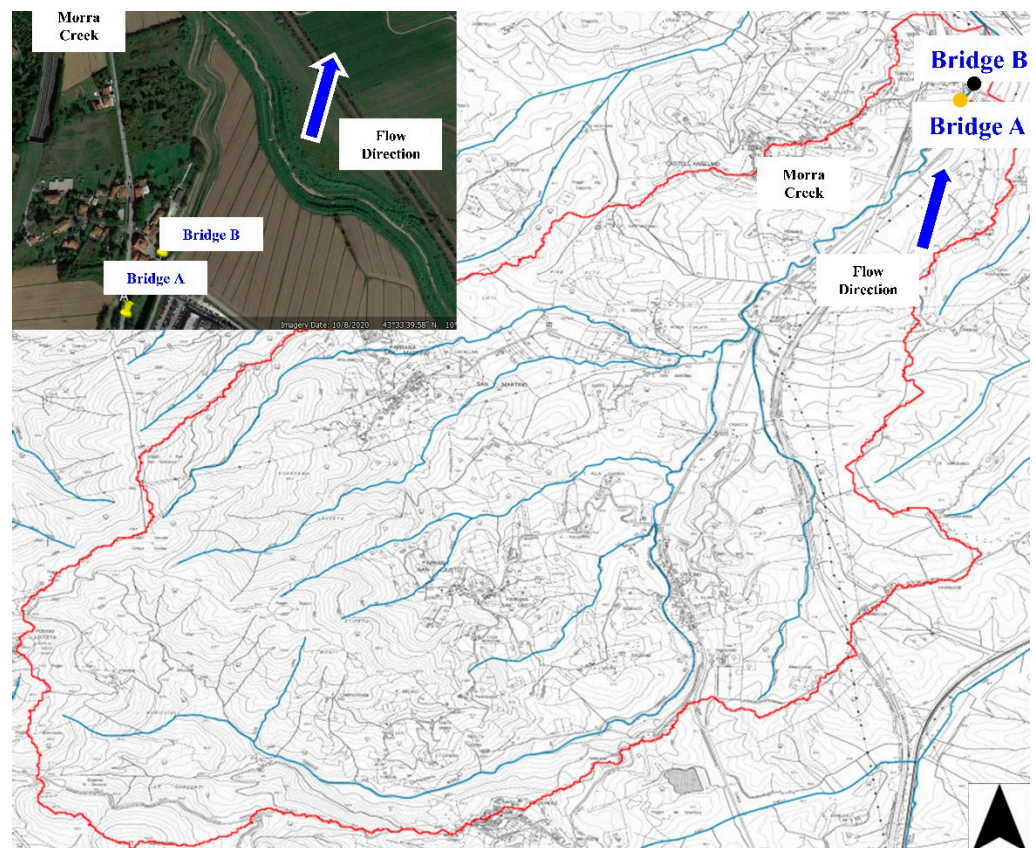
Figure 2. Morra Basin overview and locations of "Bridge A" and "Bridge B" cross-sections (yellow and black filled circles) along Morra Creek (soft blue line). The blue arrow indicates the flow direction.

In the last 30 years of hydraulic and hydrological observations, the largest flood was recorded in September 2017 when 250 mm of rain fell in three hours within the Morra Basin watershed. The hydraulic risk is due to the restriction at "Bridge B" cross-section of Morra Creek vegetated river.

Figure 3a shows the Morra Creek hydraulic conditions during September 2017 flood, whilst Figure 3b,c report a view of "Bridge A" (43°33′23″ N–10°28′41″ E) and "Bridge B" (43°33′26″ N–10°28′44″ E) structures and cross-sections, respectively.

2.2. 1D and 2D Hydraulic Simulations

In the present study, the hydraulic efficiency in reducing both peak discharge and water level at "Bridge B" cross-section of Morra Creek was analyzed and discussed, based on the proposal of two different green–blue flood control scenarios, here respectively referred to as green–blue scenario I and green–blue scenario II. In the first scenario (green–blue scenario I), a diffuse lamination effect was modeled and simulated within Morra Creek, as an innovative proposal of environment-friendly management practice of the riverine common reed beds. In the second case (green–blue scenario II), riverine vegetation was modeled to be at its current phenological development stage and flood mitigation was simulated by considering two vegetated flood control areas first and then just a deeper single vegetated flood control area.

All the hydraulic simulations were conducted with HEC-RAS v5.0 freeware software under unsteady flow conditions, aiming at evaluating the flooding lamination effects along the entire vegetated river over time. In detail, for green–blue scenario I, only 1D geometric and numerical schemes were adopted. In contrast, in the case of green–blue scenario II, a 1D scheme was employed to simulate flow along Morra Creek, and 2D geometric and numerical schemes were considered for simulating the vegetated flood control areas (e.g., customized meshes). The effects of the two Green-Blue flood mitigation scenarios proposed

in the present study were quantitatively evaluated for an input flow based on ahydrological hydrograph characterized by a return period T of 200 years.
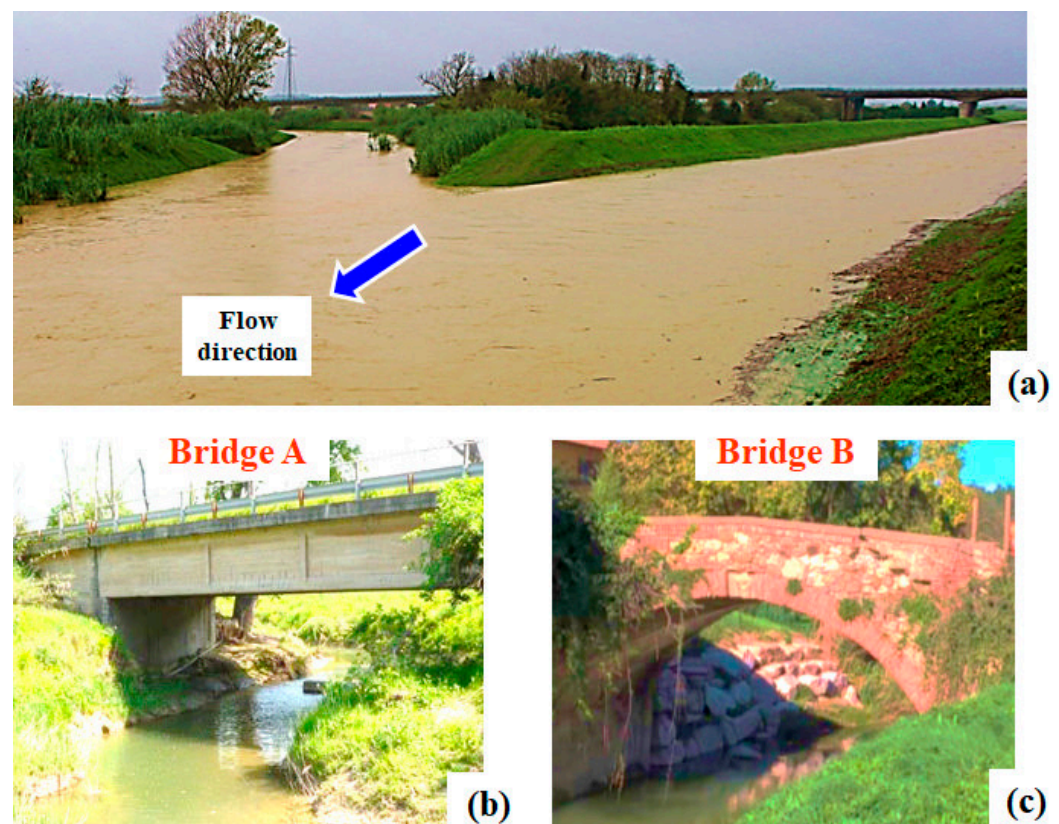

Figure 3. (**a**) Effects of the September 2017 flooding event on Morra Creek hydraulic conditions. The blue arrow indicates the flow direction. Detailed views of (**b**) "Bridge A" (43°33′23″ N–10°28′41″ E) and (**c**) "Bridge B" (43°33′26″ N–10°28′44″ E) cross-sections and structures.

The dimensional features of "Bridge A" and "Bridge B" structures and cross-sections were reproduced in the HEC-RAS v5.0 geometric model. In particular, the spans of the two bridges were modeled to evaluate the effective flood peak reduction efficiencies for the two green–blue flood control scenarios herein proposed, in terms of peak water level and discharge values.

The "Bridge A" and "Bridge B" actual geometries are summarized in Tables 1 and 2.

Table 1. "Bridge A" geometry and dimensions: height from Morra Creek bed (m), span width (m), and length (m).

Span Features	Dimensions (m)
Height	4.40
Width	18.55
Length	10.38

Table 2. "Bridge B" geometry and dimensions: height from Morra Creek bed (m), span width (m), and length (m).

Span Features	Dimensions (m)
Height	4.50
Width	8.07
Length	5.23

Figure 4a displays the HEC-RAS v5.0 geometry model of Morra Creek vegetated river, adopted here for running the initial 1D hydraulic simulation. In the present numerical study, "Bridge A" and "Bridge B" cross-sections are indicated as "3019.5" (white unfilled circle) and "3015.3" (blue unfilled circle), respectively. As shown in Figure 4b,c, "Bridge A" and "Bridge B" geometries and cross-sections were modeled and then simulated here to assess the hydraulic efficiency of the two examined green–blue scenarios in reducing water level and discharge flood peaks under unsteady flow conditions.
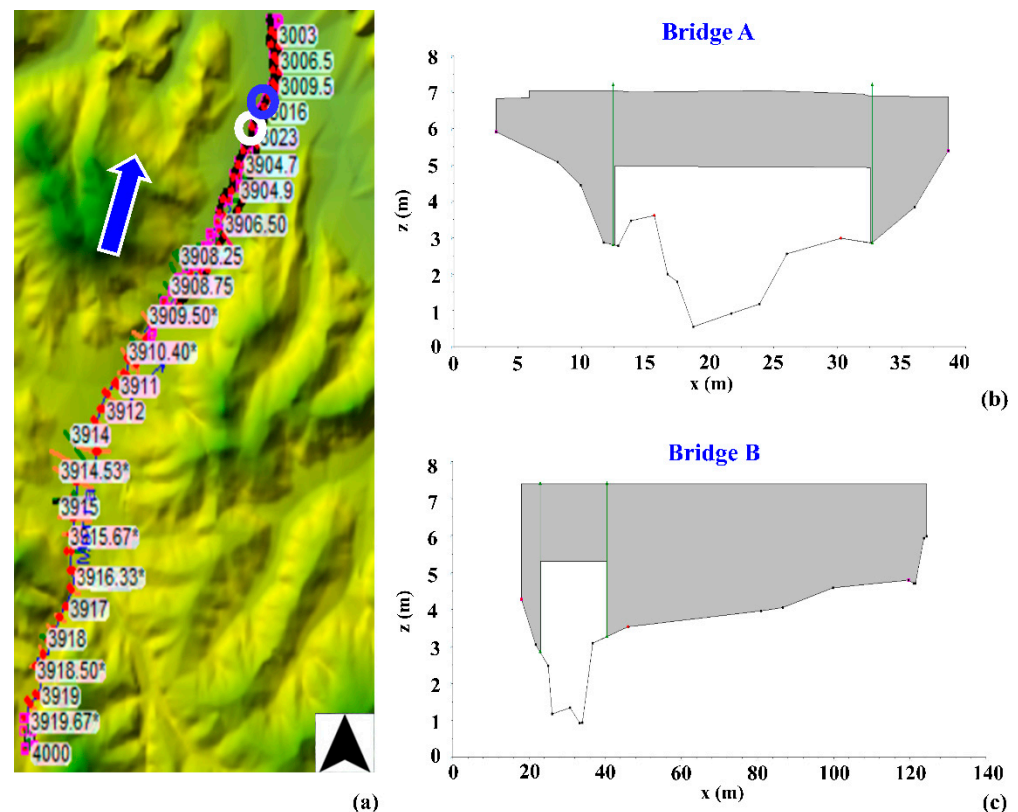

Figure 4. (**a**) Morra Creek HEC-RAS v5.0 geometry model of the 1D unsteady hydraulic simulations for Scenario I. The * in the figure is just due to the software output visualization. Scheme of (**b**) "Bridge A" (white circle in Figure 4a) and (**c**) "Bridge B" (blue circle in Figure 4a) cross-sections adopted in HEC-RAS v5.0 geometry model. The blue arrow indicates the flow direction.

Figure 5 shows the Morra Creek known hydrological hydrograph for a return period T of 200 years, having a peak discharge of 155.15 $m^3 \ s^{-1}$.

To properly model and analyze the actual ecohydraulic conditions observed within Morra Creek, upstream of "Bridge A" cross-section, values of Manning's n hydraulic roughness coefficients equal to 0.05 $m^{-1/3}$ s (rocks and very low common reed plants) and 0.06 $m^{-1/3}$ s (very low grassy shrubs) were employed here to simulate hydraulic roughness at both riverbed and floodplain stages, respectively. Instead, downstream of "Bridge A" cross-section, a value of Manning's n equal to 0.033 $m^{-1/3}$ s was adopted for Morra Creek riverbed, where the whole bottom was cleaner and straighter and to 0.04 $m^{-1/3}$ s at the floodplains, where it was possible mostly observing short vegetation related to agricultural cultivation.

As reported in the next section, the main morphometric and phenological features of the riverine vegetation species identified along Morra Creek were rigorously analyzed to define the most suitable values of Manning's n hydraulic roughness coefficients to be employed in the hydraulic simulations performed in the case of the green–blue Scenario I for properly representing the evolutive trends of the riverine vegetation canopy analyzed in the present study case.
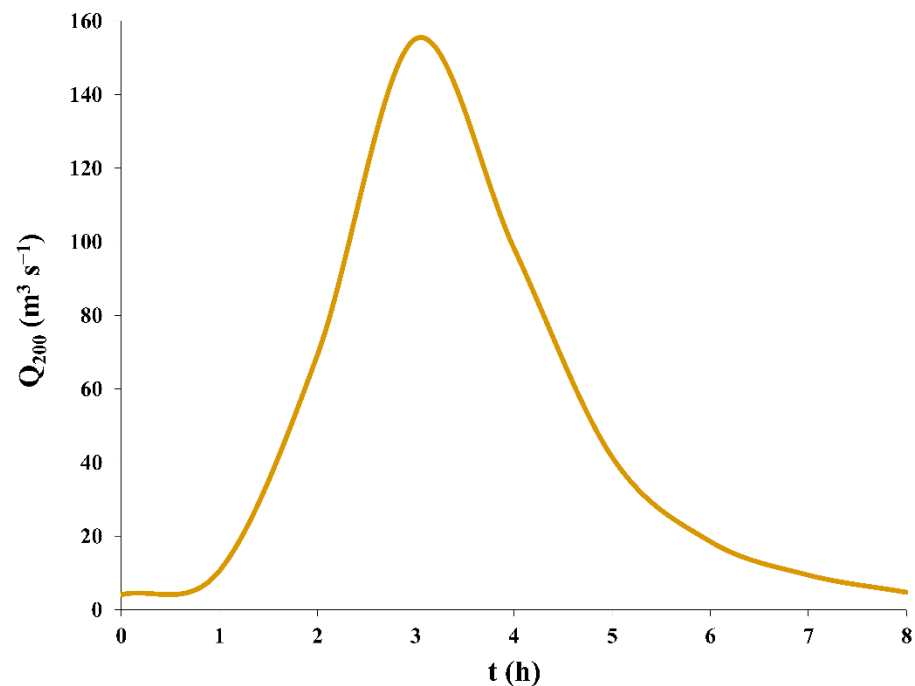
Figure 5. Hydrological hydrograph for Morra Creek associated with a return period T of 200 years, indicated in the present study as Q_{200} (m^3 s^{-1}) and t (h) is the time.

2.3. Green–blue Flood Control Scenario I

Riverine Vegetation Growth

The only riverine vegetation species recognized across the vegetated stream examined in the present study is a weed species named *Phragmites australis* (Cav.) Trin. Ex. Steudel., most known as common reed beds.

As depicted in Figure 6, increasing values of Manning's n coefficients were considered for the green–blue scenario I to simulate the growth in biomass area of the examined common reed beds (indicated by the green-yellow rectangles in Figure 6) along Morra Creek, corresponding to an augmentation in leaf area index (LAI), precisely defined as the ratio between the total leaf area distributed on the riverine plants' height (in m^2) and the projected ground area (in m^2) in the field [12,31,38,39].

As suggested by many previous analytical and modeling studies on the real-scale ecohydrodynamic response of common reed stands [11,40,41], the vertical distribution of plants' green leaf volumes is very similar on the whole reed height, with negligible LAI values in the first 0.10–0.15 m from the ground [38,41]. Thus, LAI is rigorously the same as plant area index (PAI) in the case of common reed beds, with PAI quantitatively obtained by dividing the total stems and leaves areas (in m^2) within the examined riverine plants' height (in m^2) and the projected ground area (in m^2), both measured in dedicated ecohydraulic field campaigns [42,43].

In the present study, to properly consider the actual phenological and morphometric processes associated with riverine vegetation canopy traits in the hydraulic simulations, overall Morra Creek's hydraulic roughness was modeled in the case of green–blue scenario I by considering increasing Manning's n values ranging from 0.05 m$^{-1/3}$ s (no vegetation cover) to 0.40 m$^{-1/3}$ s (massive common reed cover), to assess the flood peak control efficiencies associated with a diffuse augmentation in hydraulic roughness due to the only common reed beds' growth. Thus, for green–blue scenario I, the hydraulic simulations aimed at identifying the minimum value of Manning's n hydraulic roughness coefficient corresponding to a surface water elevation (SWE, m a.m.s.l.) value compatible with span height at "Bridge B" cross-section, equal to 4.50 m (See Table 2).
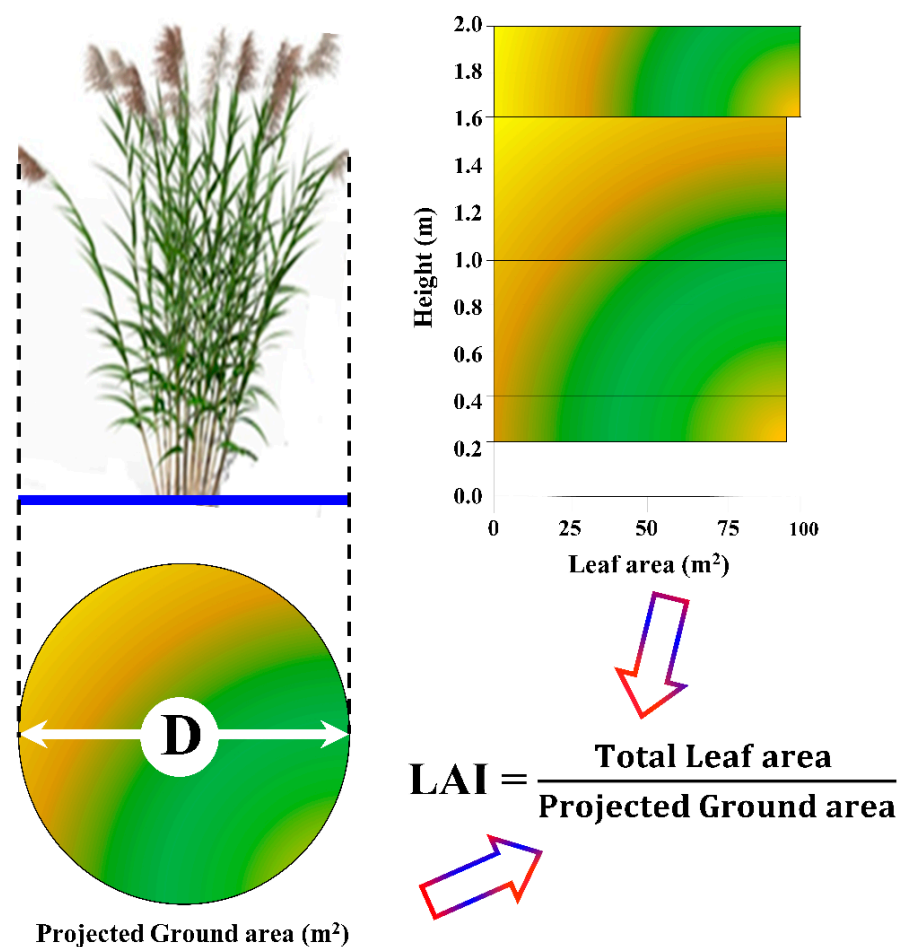
Figure 6. Vertical distribution of riverine vegetation's leaf area for 2 m high plants (green-yellow rectangles) and corresponding leaf area index (LAI) in the case of the riverine vegetation species identified along the Morra Creek: *Phragmites australis* (Cav.) Trin. Ex. Steudel. (common reed stands); D (m) is the average diameter of the "Projected ground area" (m²).

A total of twenty 1D unsteady hydraulic simulations were carried out for green–blue scenario I, by applying an increase of 0.02 $m^{-1/3}$ s to Manning's n hydraulic roughness coefficient at each HEC-RAS v5.0 run.

2.4. Green–Blue Flood Control Scenario II

The HEC-RAS v5.0 geometry model adopted in the 2D hydraulic simulation is reported in Figure 7a, with FC_{A1} and FC_{A2} representing here two vegetated flood control areas located at Morra Creek left and right orographic banks, respectively (indicated in Figure 7a by the green polygons). In detail, FC_{A1} and FC_{A2} are two agricultural areas, to be employed here as vegetated flood control areas, representing a proposal of engineering solution based on a perspective of low environmental and ecological impacts. The 2D unsteady hydraulic simulation was first carried out by connecting the 2D geometry networks of FC_{A1} and FC_{A2} vegetated flood control areas to the 1D geometry model through side green structures to allow the bidirectional exchange of water volumes between the 1D and the 2D geometry models.
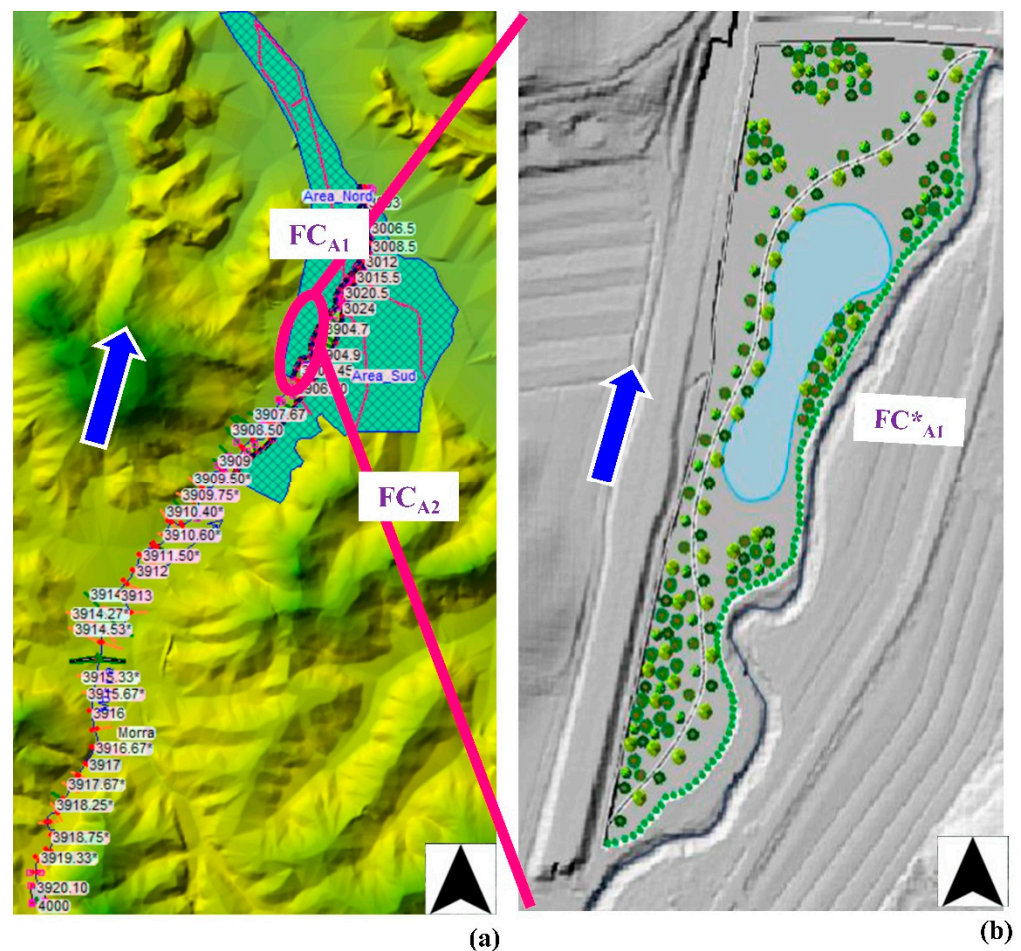
Figure 7. (**a**) HEC-RAS v5.0 geometry models associated with Morra Creek and the two vegetated flood control areas indicated as FC_{A1} and FC_{A2} adopted in green–blue scenario II. The * in the figure is just due to the software output visualization. (**b**) View of the single flood control area $FC*_{A1}$, representing an alternative solution to FC_{A1} and FC_{A2} areas. The blue arrow indicates the flow direction.

To exclude the riverine vegetation growth from the 2D hydraulic simulations associated with Morra Creek in the green–blue scenario II, a value of Manning's n coefficient of 0.05 $m^{-1/3}$ s was assigned to the whole vegetated water body to simulate the total riverine vegetation removal along the vegetated river examined in the present study. As indicated in Figure 7b, a further 2D hydraulic simulation was carried out by replacing the two vegetated flood control areas FC_{A1} and FC_{A2} areas with a single area, indicated here as $FC*_{A1}$, narrower and 2 m deeper than the original FC_{A1}, to evaluate its hydraulic efficiency in achieving the desired peak reduction effect for both discharge and water level values at "Bridge B" cross-section of Morra Creek.

As shown in Figure 7b, the proposal to realize a natural wet area and the planting of trees and shrubs buffer strips or riparian hygrophilous plants would result in eco-friendly and sustainable protection of water resources quality and, therefore, in the contemporary improvement of the ecological services associated with the presence of the single vegetated flood control area $FC*_{A1}$.

The following Table 3 summarizes the main dimensional features of $FC*_{A1}$. Width and depth are indicated here as average values.

Table 3. Main dimensional features of the vegetated flood control area FC*$_{A1}$: volume (m^3), average depth (m), length (m) and average width (m).

FC*$_{A1}$ Feature	Value
Volume (m^3)	8.02×10^3
Depth (m)	1.26
Length (m)	730
Width (m)	105

In Table 4 are reported the most relevant numerical features of the 1D and 2D unsteady hydraulic simulations carried out in the present study for the two green–blue flood control scenarios.

Table 4. Main features of the unsteady hydraulic simulations performed here: Scenarios, numerical scheme, number of simulations, here indicated as runs.

Scenario	Scheme	Runs
Current ecohydraulic conditions	1D	1
Green–blue scenario I	1D	20
Green–blue scenario II	1D + 2D (2 areas)	1
	1D + 2D (1 area)	1

2.5. Flood Control Efficiency: Peak Discharge and Water Level Reduction

As remarked by Del Giudice et al. [44] among others, the hydraulic efficiencies (expressed here in percentage, %) of the flood control effects corresponding to both green–blue scenario I and green–blue scenario II in terms of peak discharge Q (m^3 s^{-1}) and water level h (m) reduction associated with a return period T of 200 years, were quantitively computed as follows:

$$\eta\ (\%) = (peak_{in} - peak_{out})/peak_{in}, \tag{1}$$

where $peak_{in}$ and $peak_{out}$ indicate, respectively, the peak discharge Q (m^3 s^{-1}) and water level h (m) peak values in input and output at "Bridge B" cross-section of Morra Creek for a return period T of 200 years. The corresponding peak reduction efficiencies are here indicated as η_Q (%) and η_h (%), respectively.

3. Results

3.1. Morra Creek Current Ecohydraulic Conditions

The flooding outcomes resulting from the 1D unsteady hydraulic simulation of the actual Morra Creek ecohydraulic conditions are displayed in Figure 8a,b, representing, respectively, surface water elevation (SWE) and flow average velocities U (m s^{-1}) at each Morra Creek cross-section identified in the HEC-RAS v5.0 geometry model, for a hydrological hydrograph based on a return period T of 200 years, indicated in the present study as Q_{200} (m^3 s^{-1}).

As it emerges from the analysis of Figure 8a, the water level value at "Bridge B" cross-section of Morra Creek resulting from the 1D unsteady hydraulic simulation under the actual riverine vegetation conditions is equal to approximately 6.50 m, which is higher than "Bridge B" span height, equal to 4.50 m, as shown in Table 2. Thus, both green–blue scenario I and green–blue scenario II were modeled and then simulated in the following sections aiming at reducing the hydrological peaks for T of 200 years at "Bridge B" cross-section of Morra Creek.
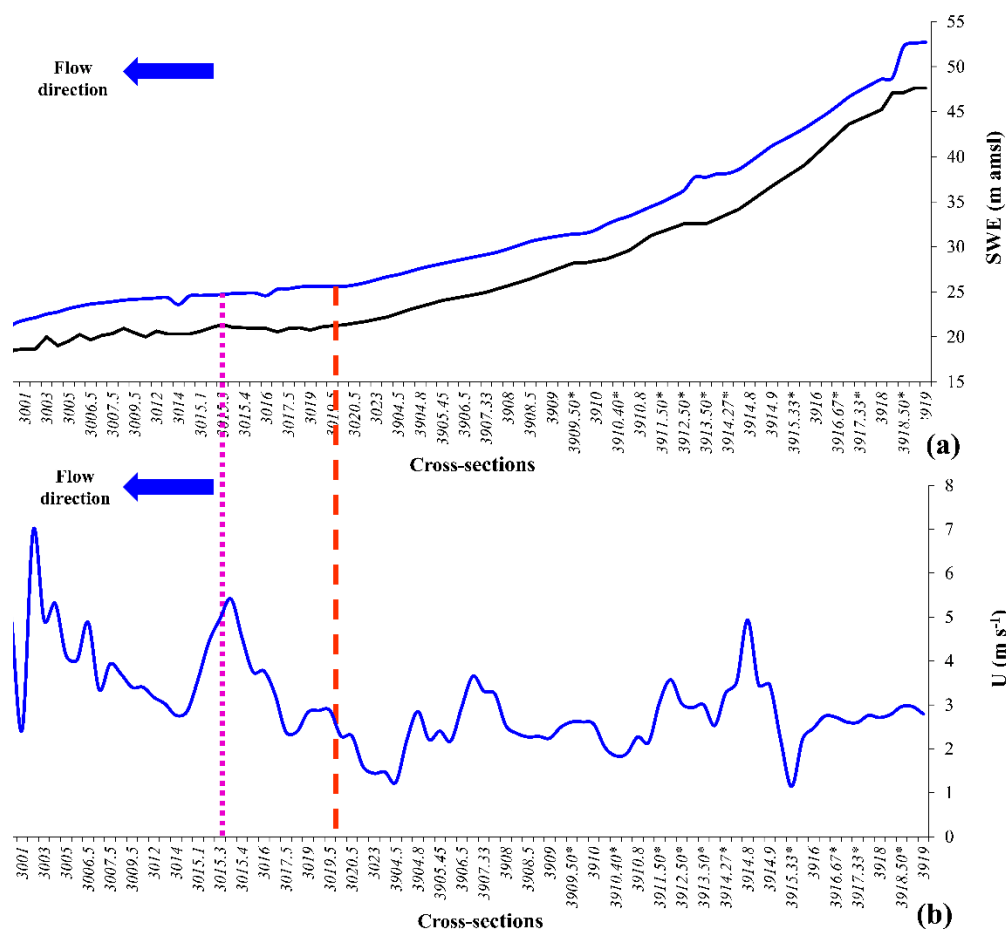
Figure 8. (**a**) Surface Water Elevation SWE (m a.m.s.l.) and (**b**) Flow average velocities U (m s^{-1}) at Morra Creek cross-sections resulting from the 1D unsteady simulation. The continuous black line represents the Morra Creek bed elevation. The blue arrow indicates the flow direction, while the orange dashed lines and the purple dotted lines respectively indicate the locations of "Bridge A" and "Bridge B" cross-sections. The * in the figure is just due to the software output visualization.

3.2. Green–Blue Flood Control Scenario I

In Figure 9a,b are, respectively, displayed the values in percentage of peak discharge Q (m^3 s^{-1}) and water level h (m) reduction efficiencies associated with T = 200 years for green–blue Scenario I at "Bridge B" cross-section, as a function of the increasing Manning's n coefficients values reproducing the real-scale augmentation in LAI values characterizing the riverine vegetation stands examined in the present study. In detail, both Figure 9a,b were obtained through twenty 1D unsteady hydraulic simulations (see Table 4).

As expected, it is possible to observe, in Figure 9a,b, that for green–blue scenario I, the peak reduction efficiencies in terms of both peak discharge and water level values at "Bridge B" cross-sections increase with common reed biomass growth over Morra Creek vegetated river, according to two very similar trends. In detail, η_{Q_I} values vary from 28.35% to 29.70%, while η_{h_I} ones vary from 25.09% to 31.46%. These values indicate that η_{h_I} is slightly more sensitive than η_{Q_I} to the real-scale changes in Manning's n hydraulic roughness coefficients, corresponding to the phenological evolutive trend of riverine common reed beds under their natural conditions across the whole length of the vegetated watercourse.
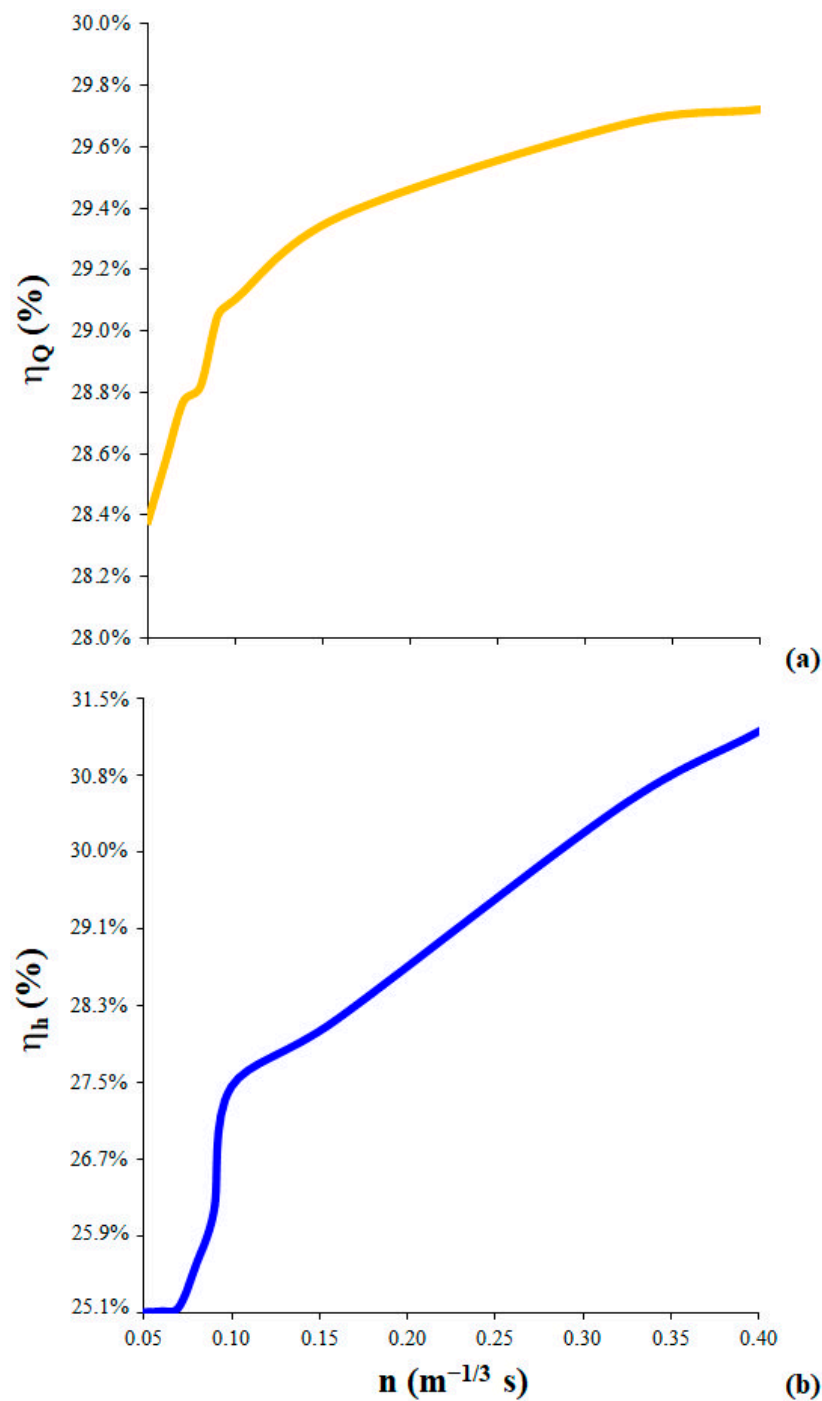
Figure 9. Flood peak (**a**) discharge Q (m^3 s^{-1}) (yellow line) and (**b**) water level h (m) (blue line) reduction efficiencies (in percentage, %) computed at "Bridge B" cross-section of Morra Creek, as a function of Manning's n ranging between 0.05 m$^{-1/3}$ s (no Common reed cover) and 0.40 m$^{-1/3}$ s (massive Common reed cover), respectively indicated as η_{QI} (%) and η_{hI} (%).

3.3. Green–Blue Flood Control Scenario II

Figure 10a,b illustrate, respectively, the outcomes of the 2D unsteady simulation in terms of SWE (m a.m.s.l.) for the whole Morra Creek length (Figure 10a), originally considered in green–blue scenario II and a detailed view of the two vegetated flood control areas FC$_{A1}$ and FC$_{A2}$ (Figure 10b).
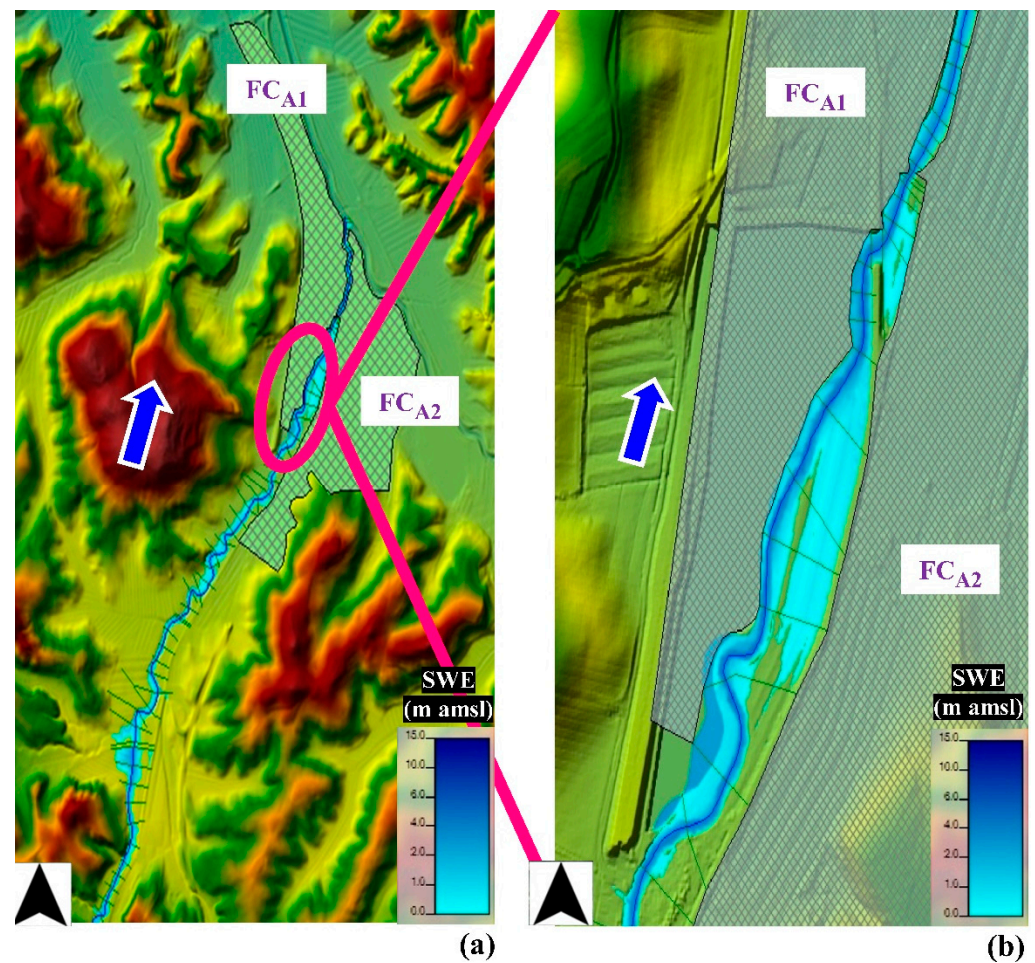
Figure 10. (**a**) Surface water elevations SWE (m a.m.s.l.) outcoming from the 2D unsteady simulation for Morra Creek. (**b**) Detailed view of the two vegetated flood control areas FC_{A1} and FC_{A2}, and corresponding SWE (m a.m.s.l.). The blue arrow indicates the flow direction, while the two soft green polygons represent respectively the modeled flood control areas FC_{A1} and FC_{A2}.

The results of the 2D hydraulic simulation reported in Figure 10a,b show that the combined action of the two vegetated flood control areas FC_{A1} and FC_{A2} was not sufficient for reducing peak SWE (m a.m.s.l.) at the examined "Bridge B" cross-section, equal to 6.0 m, indicating the need for replacing FC_{A1} and FC_{A2} areas with the only vegetated flood control area FC^*_{A1} in the further 2D hydraulic model and simulation.

In Figure 11a,b, the HEC-RAS v5.0 geometry model and the flooding outcomes are shown, resulting from the 2D hydraulic simulation implemented here for green–blue scenario II in terms of SWE (m a.m.s.l.), by considering the only single vegetated flood control area FC^*_{A1}.

It emerges from the analyses of Figure 11a,b that for green–blue scenario II the surface water elevations SWE (m a.m.s.l.) is equal to 4.04 m, which is quantitatively compatible with "Bridge B" span height, equal to 4.50 m. These trends can also be easily observed by analyzing the effects on the overall flood risk assessment of the flooding outcomes computed along the Morra Creek cross-sections through the 2D unsteady hydraulic simulation, displayed in Figure 12a,b. In detail, in Figure 12a,b the values of SWE (m a.m.s.l.) and flow average velocities U (m s^{-1}) at each modeled and then simulated Morra Creek cross-sections, respectively.

In Table 5 are indicated the discharge Q_{II} (m^3 s^{-1}) and water level h_{II} (m) values of the output hydrograph of the 2D unsteady hydraulic simulation at "Bridge B" cross-section of

Morra Creek for green–blue scenario II because of the existence of the only vegetated flood control area FC*$_{A1}$.

Table 5. Discharge $Q_{II,}$ (m^3 s^{-1}) and water level $h_{II,}$ (m) values for the green–blue flood control scenario II at "Bridge B" cross-section and t (h) is the time from the beginning of the output hydrograph.

t (h)	Q_{II} (m^3 s^{-1})	h_{II} (m)
0	3.41	1.03
1	9.32	1.64
2	68.47	2.76
3	109.53	4.04
4	97.14	3.93
5	40.66	2.39
6	17.39	2.05
7	9.22	1.99
8	4.68	1.01

It is possible to observe from Table 5 that, given the presence of the single vegetated flood control area FC*$_{A1}$, the value of peak discharge Q_{II} (m^3 s^{-1}) at "Bridge B" cross-section moved from 155.15 to 109.53 m^3 s^{-1}, while the value of peak water level h_{II} (m) effectively decreased from 6.50 to 4.04 m.
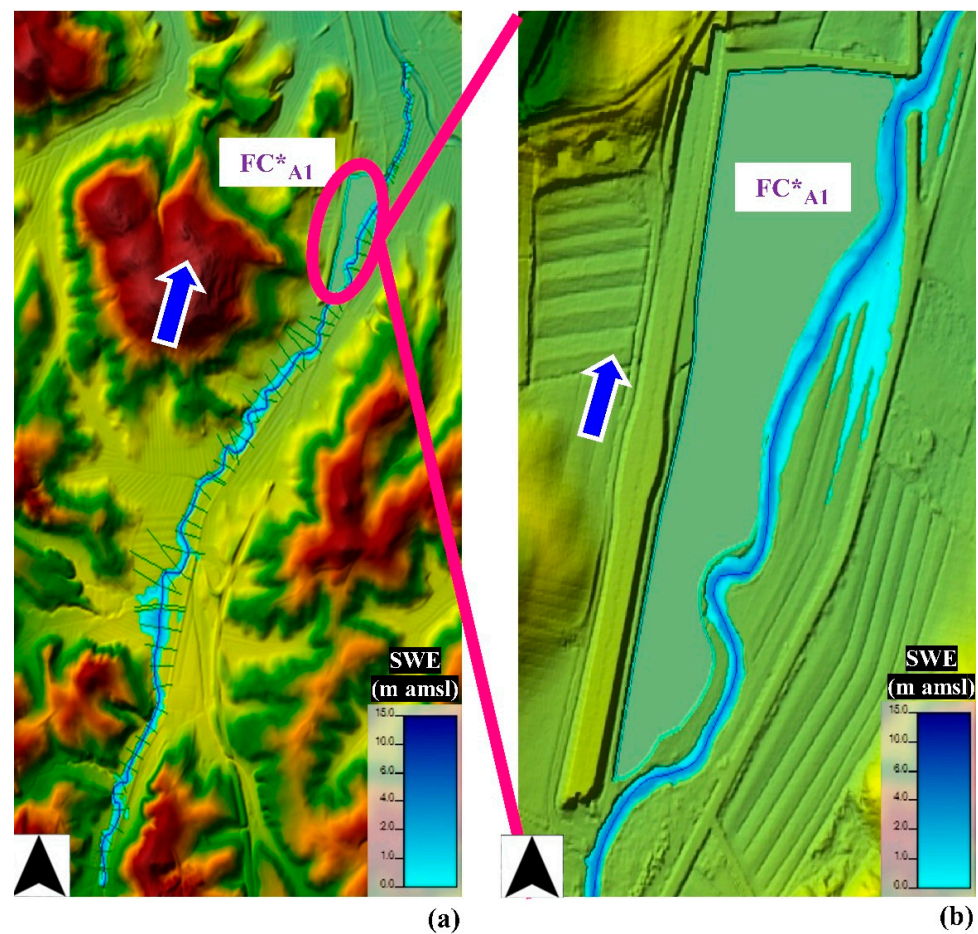

Figure 11. (**a**) Surface water elevations SWE (m a.m.s.l.) outcoming from the 2D unsteady simulation for Morra Creek, obtained by considering the only vegetated flood control area FC*$_{A1}$. (**b**) Detailed view of FC*$_{A1}$ area model, and corresponding SWE (m a.m.s.l.). The blue arrow indicates the flow direction.
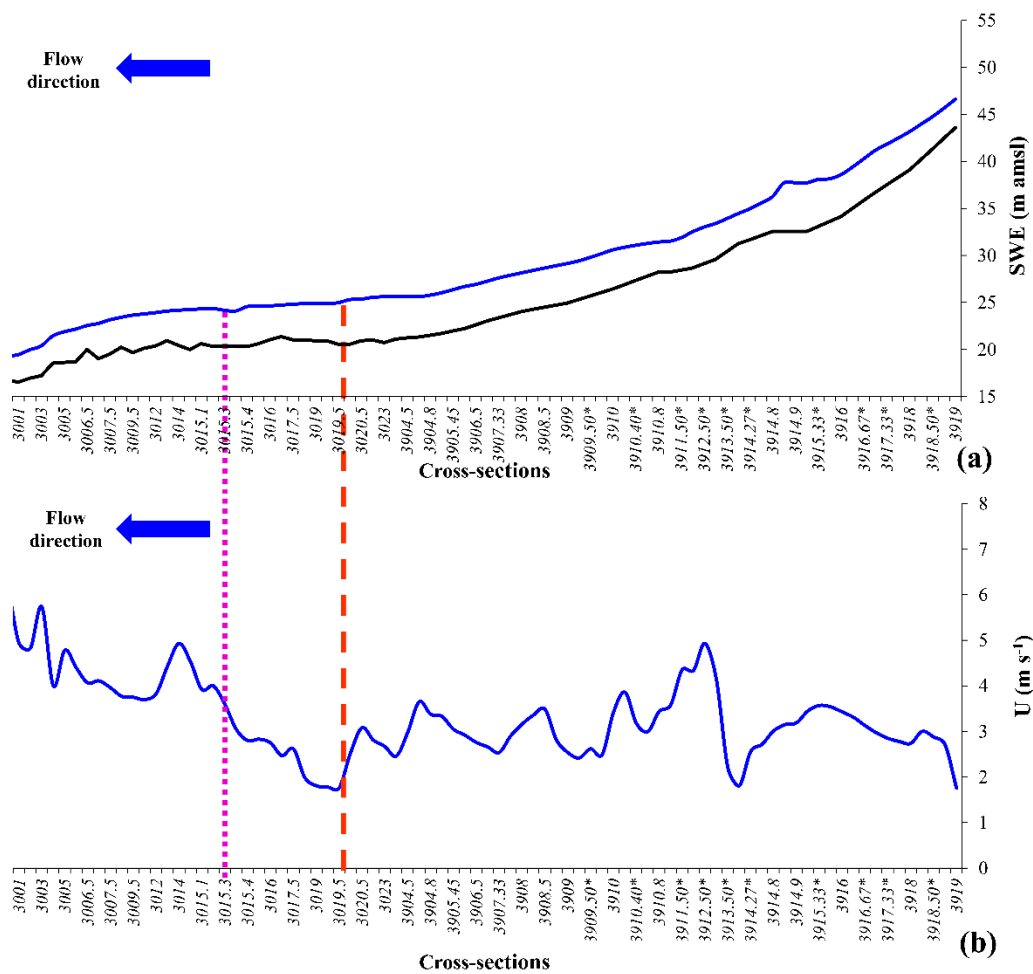
Figure 12. (**a**) Surface water elevation (SWE) and (**b**) flow average velocities U along the Morra Creek cross-sections resulting from the 2D unsteady simulation. The continuous black line represents Morra Creek bed elevation. The blue arrow indicates the flow direction, while orange dashed lines and purple dotted lines, respectively, indicate the locations of "Bridge A" and "Bridge B" cross-sections. The * in the figure is just due to the software output visualization.

4. Discussion

Based on the two green–blue flood control scenarios herein proposed, the results of the present study in terms of peak discharge and water level control effects for Morra Creek well demonstrated that both of them are capable of obtaining a satisfactory flood risk mitigation, with low ecological and environmental impacts compared to grey—or structural—hydraulic engineering solutions.

Values of Manning's n coefficients, ranging between 0.10 $m^{-1/3}$ s and 0.40 $m^{-1/3}$ s, are highly comparable with those obtained by the two previous ecohydraulic studies performed by Liu and Shan [45] and Lama et al. [46], which analyzed the average and turbulent fluctuations of flow velocity fields experimentally measured in vegetated streams to evaluate the main field-scale hydraulic and hydrodynamic effects of the riverine vegetation stands' phenology on the hydraulic conveyance of real vegetated water bodies. Both studies were carried out at increasing discharge and water levels. In the study of Liu and Shan [45], the values of Manning's n coefficients ranged from 0.12 $m^{-1/3}$ s to 0.36 $m^{-1/3}$ s, while they varied between 0.27 $m^{-1/3}$ s and 0.49 $m^{-1/3}$ s in the study carried out by Lama et al. [46].

In addition, it is important to emphasize here that Manning's n coefficient values resulting from the 1D hydraulic simulations (0.10-0.40 $m^{-1/3}$ s) well represent the actual vegetative flow resistance induced by patchy riverine vegetation, as reported by the previous ecohydraulic studies carried out by West et al. [47] and Zhu et al. [48]. Their works,

respectively, modeled the impacts of real-scale riverine vegetation distribution on water level argumentation and hydrodynamic dispersion within vegetated open channels under different growth conditions of riverine plants in both flume laboratory and field-scale study cases.

It is crucial to highlight that the outcomes of the present study refer to a single riparian vegetation species (common reed beds), while, in a more realistic perspective, the combined effect of two or more species represent a source of uncertainty which inevitably propagates in the vegetative Manning's n hydraulic roughness coefficient associated with each simulated cross-section, quantitatively varying in a wider range of values. Thus, this uncertainty could be reduced by implementing more complex and rigorous numerical analyses, obtained by coupling high-performance computational fluid dynamics (CFD) models [49–53] and simulations [54–61] with the most advanced remote sensing techniques of fluvial hydraulics, agro-forestry and land use governance interest [62–71].

5. Conclusions

From the analysis and the discussion of the outcomes of this study was possible to observe that green–blue scenario I, obtained by considering the diffuse peak lamination effect associated with common reed beds' growth along the whole Morra Creek vegetated watercourses, constitutes a valuable alternative to the fairly more impacting green–blue scenario II proposal.

In addition, it emerges that the proposals of green–blue scenarios in both urban and agricultural areas effectively constitute decisive steps in the definition of a new engineering and scientific methodology for flooding risk control associated with vegetated rivers with low ecological and environmental impacts [72–76], preserving their riverine and riparian ecosystems.

It is possible to assess that the main findings of the hydraulic simulations performed in the present study represent a useful tool for ecohydrological and ecohydraulic forecasters and modelers for flood risk control associated with both urban and agro-forestry territories.

Author Contributions: Conceptualization, G.F.C.L.; methodology, G.F.C.L., M.R.M.G. and A.E.; validation, G.F.C.L., A.E., G.B.C. and F.P.; investigation, G.F.C.L., M.R.M.G., A.E., S.M. and R.P.; data curation, G.F.C.L., M.R.M.G., A.E., S.M. and R.P.; writing—original draft preparation, G.F.C.L., M.R.M.G., A.E., S.M. and R.P.; writing—review and editing, G.F.C.L., M.R.M.G., A.E., S.M., G.B.C. and F.P. All authors have read and agreed to the published version of the manuscript.

Institutional Review Board Statement: Not applicable.

Informed Consent Statement: Informed consent was obtained from all subjects involved in the study.

Data Availability Statement: The data presented in this study are available on request from the corresponding author.

Conflicts of Interest: The authors declare no conflict of interest.

References

1. Mazzeo, F.C.; Arienzo, I.; Aulinas, M.; Casalini, M.; Di Renzo, V.; D'Antonio, M. Mineralogical, geochemical and isotopic characteristics of alkaline mafic igneous rocks from Punta delle Pietre Nere (Gargano, Southern Italy). *Lithos* **2018**, *308–309*, 316–328. [CrossRef]
2. Inzunza, D.A.; Montalva, G.A.; Leyton, F.; Prieto, G.; Ruiz, S. Shallow Ambient-Noise 3D Tomography in the Concepción Basin, Chile: Implications for Low-Frequency Ground Motions. *Bull. Seism. Soc. Am.* **2018**, *109*, 75–86. [CrossRef]
3. Santangelo, N.; Forte, G.; De Falco, M.; Chirico, G.B.; Santo, A. New insights on rainfall triggering flow-like landslides and flash floods in Campania (Southern Italy). *Landslides* **2021**, *18*, 2923–2933. [CrossRef]

4. Lama, G.F.C.; Sadeghifar, T.; Torabi Azad, M.; Sihag, P.; Kisi, O. Wind Wave Heights over the Southern Coasts of Caspian Sea: A Real-scale Comparative Analysis. *Ocean Eng.* **2021**. under review.

5. Fusco, F.; Mirus, B.B.; Baum, R.L.; Calcaterra, D.; De Vita, P. Incorporating the Effects of Complex Soil Layering and Thickness Local Variability into Distributed Landslide Susceptibility Assessments. *Water* **2021**, *13*, 713. [CrossRef]

6. Lama, G.F.C.; Sadeghifar, T.; Sihag, P.; Bayram, A.; Kisi, O. Performance of soft-computing models in predicting wave heights in complex sea flows: Case study of Persian Gulf. *Ocean Eng.* **2021**. under review.

7. Padulano, R.; Lama, G.F.C.; Rianna, G.; Santini, M.; Mancini, M.; Stojiljkovic, M. Future rainfall scenarios for the assessment of water availability in Italy. In Proceedings of the 2020 IEEE International Workshop on Metrology for Agriculture and Forestry (MetroAgriFor), Trento, Italy, 4–6 November 2020; pp. 241–246. [CrossRef]

8. Johnston, A.S.A.; Meade, A.; Ardö, J.; Arriga, N.; Black, A.; Blanken, P.D.; Bonal, D.; Brümmer, C.; Cescatti, A.; Dušek, J.; et al. Temperature thresholds of ecosystem respiration at a global scale. *Nat. Ecol. Evol.* **2021**, *5*, 487–494. [CrossRef] [PubMed]

9. Brenna, A.; Surian, N.; Ghinassi, M.; Marchi, L. Sediment–water flows in mountain streams: Recognition and classification based on field evidence. *Geomorphology* **2020**, *371*, 107413. [CrossRef]

10. Manfreda, S.; Miglino, D.; Albertini, C. Impact of detention dams on the probability distribution of floods. *Hydrol. Earth Syst. Sci. Discuss.* **2021**, *25*, 4231–4242. [CrossRef]

11. Francalanci, S.; Paris, E.; Solari, L. On the vulnerability of woody riparian vegetation during flood events. *Environ. Fluid Mech.* **2020**, *20*, 635–661. [CrossRef]

12. Errico, A.; Lama, G.F.C.; Francalanci, S.; Chirico, G.B.; Solari, L.; Preti, F. Flow dynamics and turbulence patterns in a drainage channel colonized by common reed (*Phragmites australis*) under different scenarios of vegetation management. *Ecol. Eng.* **2019**, *133*, 39–52. [CrossRef]

13. Poggi, D.; Porporato, A.; Ridolfi, R.; Albertson, J.D.; Katul, G.G. The effect of vegetation density on canopy sub-layer turbulence. *Bound. Layer Meteorol.* **2004**, *111*, 565–587. [CrossRef]

14. Västilä, K.; Järvelä, J.; Aberle, J. Characteristic reference areas for estimating flow resistance of natural foliated vegetation. *J. Hydrol.* **2013**, *492*, 49–60. [CrossRef]

15. Bulat, M.; Biron, P.M.; Lacey, J.R.W.; Botrel, M.; Hudon, C.; Maranger, R. A three-dimensional numerical model investigation of the impact of submerged macrophytes on flow dynamics in a large fluvial lake. *Freshw. Biol.* **2019**, *64*, 1627–1642. [CrossRef]

16. Peruzzo, P.; De Serio, F.; Defina, A.; Mossa, M. Wave Height Attenuation and Flow Resistance Due to Emergent or Near-Emergent Vegetation. *Water* **2018**, *10*, 402. [CrossRef]

17. Lama, G.F.C.; Errico, A.; Francalanci, S.; Solari, L.; Preti, F.; Chirico, G.B. Comparative analysis of modeled and measured vegetative Chézy's flow resistance coefficients in a drainage channel vegetated by dormant riparian reed. In Proceedings of the International IEEE Workshop on Metrology for Agriculture and Forestry, Portici, Italy, 24–26 October 2019; pp. 180–184. [CrossRef]

18. De Paola, F.; Ranucci, A. Analysis of spatial variability for stormwater capture tank assessment. *Irrig. Drain.* **2012**, *61*, 682–690. [CrossRef]

19. Večeřa, M.; Axmanová, I.; Padullés Cubino, J.; Lososová, Z.; Divíšek, J.; Knollová, I.; Aćić, S.; Biurrun, I.; Boch, S.; Bonari, G.; et al. Mapping species richness of plant families in European vegetation. *J. Veg. Sci.* **2021**, *32*, e13035. [CrossRef]

20. Ferraiuolo, R.; De Paola, F.; Fiorillo, D.; Caroppi, G.; Pugliese, F. Experimental and Numerical Assessment of Water Leakages in a PVC-A Pipe. *Water* **2020**, *12*, 1804. [CrossRef]

21. Chanson, H.; Gualtieri, C. Similitude and scale effects of air entrainment in hydraulic jumps. *J. Hydraul. Res.* **2008**, *46*, 35–44. [CrossRef]

22. Lama, G.F.C.; Errico, A.; Pasquino, V.; Mirzaei, S.; Preti, F.; Chirico, G.B. Velocity Uncertainty Quantification based on Riparian Vegetation Indices in open channels colonized by *Phragmites australis*. *J. Ecohydraulics* **2021**, 1–6. [CrossRef]

23. Latella, M.; Bertagni, M.B.; Vezza, P.; Camporeale, C. An integrated methodology to study riparian vegetation dynamics: From field data to impact modeling. *J. Adv. Model. Earth Syst.* **2020**, *12*, e2020MS002094. [CrossRef] [PubMed]

24. Stella, J.C.; Rodríguez-González, P.M.; Dufour, S.; Bendix, J. Riparian vegetation research in Mediterranean-climate regions: Common patterns, ecological processes, and considerations for management. *Hydrobiologia* **2013**, *719*, 291–315. [CrossRef]

25. De Paola, F.; Giugni, M.; Pugliese, F.; Romano, P. Optimal Design of LIDs in Urban Stormwater Systems Using a Harmony-Search Decision Support System. *Water Resour. Manag.* **2018**, *32*, 4933–4951. [CrossRef]

26. Link, O.; Sanhueza, C.; Arriagada, P.; Brevis, W.; Laborde, A.; González, A.; Wilkes, M.; Habit, E. The fish Strouhal number as a criterion for hydraulic fishway design. *Ecol. Eng.* **2017**, *103*, 118–126. [CrossRef]

27. Zou, G.; Papirio, S.; Ylinen, A.; Di Capua, F.; Lakaniemi, A.M.; Puhakka, G.A. Fluidized-bed denitrification for mine waters. Part II: Effects of Ni and Co. *Biodegradation* **2014**, *25*, 417–423. [CrossRef]

28. Pace, R.; De Fino, F.; Rahman, M.A.; Pauleit, S.; Nowak, D.J.; Grote, R. A single tree model to consistently simulate cooling, shading, and pollution uptake of urban trees. *Int. J. Biometeorol.* **2021**, *65*, 277–289. [CrossRef] [PubMed]

29. Bianco, F.; Monteverde, G.; Race, M.; Papirio, S.; Esposito, G. Comparing performances, costs and energy balance of ex situ remediation processes for PAH-contaminated marine sediments. *Environ. Sci. Pollut. Res.* **2020**, *27*, 19363–19374. [CrossRef]

30. Cioffi, B.; Ianiro, G.; Iaccarino, D.; D'Apice, F.; Ferraro, A.; Race, M.; Spasiano, D.; Esposito, E.; Monini, M.; Serra, F.; et al. A potential risk assessment tool to monitor pathogens circulation in coastal waters. *Environ. Res.* **2021**, *200*, 111748. [CrossRef] [PubMed]

31. Licciardello, F.; Sacco, A.; Barbagallo, S.; Ventura, D.; Cirelli, G.L. Evaluation of Different Methods to Assess the Hydraulic Behavior in Horizontal Treatment Wetlands. *Water* **2020**, *12*, 2286. [CrossRef]

32. Varra, G.; Pepe, V.; Cimorelli, L.; Della Morte, R.; Cozzolino, L. On integral and differential porosity models for urban flooding simulation. *Adv. Water Resour.* **2020**, *136*, 103455. [CrossRef]

33. Thiemer, K.; Schneider, S.C.; Demars, B.O.L. Mechanical removal of macrophytes in freshwater ecosystems: Implications for ecosystem structure and function. *Sci. Total Environ.* **2021**, *782*, 146671. [CrossRef]

34. Bonanomi, G.; Zotti, M.; Mogavero, V.; Cesarano, G.; Saulino, L.; Rita, A.; Tesei, G.; Allegrezza, M.; Saracino, A.; Allevato, E. Climatic and anthropogenic factors explain the variability of Fagus sylvatica treeline elevation in fifteen mountain groups across the Apennines. *For. Ecosyst.* **2020**, *7*, 5. [CrossRef]

35. Box, W.; Järvelä, J.; Västilä, K. Flow resistance of floodplain vegetation mixtures for modelling river flows. *J. Hydrol.* **2021**, *601*, 126593. [CrossRef]

36. Artini, G.; Calvani, G.; Francalanci, S.; Solari, L. Effects of vegetation at a bar confluence on river hydrodynamics: The case study of the Arno River at Greve junction. *River Res. Appl.* **2021**, *37*, 615–626. [CrossRef]

37. Peruzzi, C.; Castaldi, M.; Francalanci, S.; Solari, L. Three-dimensional hydraulic characterisation of the Arno River in Florence. *J. Flood Risk Manag.* **2019**, *12*, e12490. [CrossRef]

38. Lama, G.F.C.; Chirico, G.B. Effects of reed beds management on the hydrodynamic behaviour of vegetated open channels. In Proceedings of the 2020 IEEE International Workshop on Metrology for Agriculture and Forestry (MetroAgriFor), Trento, Italy, 4–6 November 2020; pp. 149–154. [CrossRef]

39. Maji, S.; Hanmaiahgari, P.R.; Balachandar, R.; Pu, J.H.; Ricardo, A.M.; Ferreira, R.M.L. A Review on Hydrodynamics of Free Surface Flows in Emergent Vegetated Channels. *Water* **2020**, *12*, 1218. [CrossRef]

40. Svensk, M.; Coste, S.; Gérard, B.; Gril, E.; Julien, F.; Maillard, P.; Stahl, C.; Leroy, C. Drought effects on resource partition and conservation among leaf ontogenetic stages in epiphytic tank bromeliads. *Physiol. Plant.* **2020**, *170*, 488–507. [CrossRef] [PubMed]

41. Lama, G.F.C.; Crimaldi, M.; Pasquino, V.; Padulano, R.; Chirico, G.B. Bulk Drag Predictions of Riparian *Arundo donax* Stands through UAV-acquired Multispectral Images. *Water* **2021**, *13*, 1333. [CrossRef]

42. Wang, Y.; Yin, Z.; Liu, Y. Numerical investigation of solitary wave attenuation and resistance induced by rigid vegetation based on a 3-D RANS model. *Adv. Water Resour.* **2020**, *146*, 103755. [CrossRef]

43. van Veelen, T.J.; Karunarathna, H.; Reeve, D.E. Modelling wave attenuation by quasi-flexible coastal vegetation. *Coast. Eng.* **2021**, *164*, 103820. [CrossRef]

44. Del Giudice, G.; Rasulo, G.; Siciliano, D.; Padulano, R. Combined Effects of Parallel and Series Detention Basins for Flood Peak Reduction. *Water Resour. Manag.* **2014**, *28*, 3193–3205. [CrossRef]

45. Liu, C.; Shan, Y. Analytical model for predicting the longitudinal profiles of velocities in a channel with a model vegetation patch. *J. Hydrol.* **2019**, *576*, 561–574. [CrossRef]

46. Lama, G.F.C.; Errico, A.; Francalanci, S.; Solari, L.; Preti, F.; Chirico, G.B. Evaluation of Flow Resistance Models Based on Field Experiments in a Partly Vegetated Reclamation Channel. *Geosciences* **2020**, *10*, 47. [CrossRef]

47. West, P.O.; Wallis, S.G.; Sonnenwald, F.C.; Hart, J.R.; Stovin, V.R.; Guymer, I. Modelling transverse solute mixing across a vegetation generated shear layer. *J. Hydraul. Res.* **2020**, *59*, 621–636. [CrossRef]

48. Zhu, Z.; Yang, Z.; Huai, W.; Wang, H.; Li, D.; Fan, Y. Growth-decay model of vegetation based on hydrodynamics and simulation on vegetation evolution in the channel. *Ecol. Indic.* **2020**, *119*, 106857. [CrossRef]

49. Di Cristo, C.; Iervolino, M.; Vacca, A. Applicability of Kinematic and Diffusive models for mud-flows: A steady state analysis. *J. Hydrol.* **2018**, *559*, 585–595. [CrossRef]

50. Di Nunno, F.; Granata, F.; Gargano, R.; De Marinis, G. Prediction of spring flows using nonlinear autoregressive exogenous (NARX) neural network models. *Environ. Monit. Assess.* **2021**, *193*, 350. [CrossRef]

51. Gobbetti, L.E.C. Design of the filling and emptying system of the new Panama Canal locks. *J. Appl. Water Eng. Res.* **2013**, *1*, 28–38. [CrossRef]

52. Fecarotta, O.; Messa, G.V.; Pugliese, F. Numerical assessment of the vulnerability to impact erosion of a pump as turbine in a water supply system. *J. Hydroinform.* **2020**, *22*, 691–712. [CrossRef]

53. Badas, M.G.; Rossi, R.; Garau, M. May a Standard VOF Numerical Simulation Adequately Complete Spillway Laboratory Measurements in an Operational Context? The Case of Sa Stria Dam. *Water* **2020**, *12*, 1606. [CrossRef]

54. Nicolosi, F.; Ciliberti, D.; Della Vecchia, P.; Corcione, S. Experimental analysis of aircraft directional control effectiveness. *Aerosp. Sci. Technol.* **2020**, *106*, 106099. [CrossRef]

55. Lama, G.F.C.; Crimaldi, M. Calibration of Flow Resistance Models in Vegetated Ditches Based on UAV Remote Sensing. Presented at the 1st International Electronic Conference on Agronomy, online, 3–17 May 2021; Volume 3, pp. 17–21.

56. Eke, E.; Czapiga, M.; Viparelli, E.; Shimizu, Y.; Imran, J.; Sun, T.; Parker, G. Coevolution of width and sinuosity in meandering rivers. *J. Fluid Mech.* **2014**, *760*, 127–174. [CrossRef]

57. Vettori, D.; Nikora, V. Flow–seaweed interactions: A laboratory study using blade models. *Environ. Fluid Mech.* **2018**, *18*, 611–636. [CrossRef]

58. Bahmanpouri, F.; Daliri, M.; Khoshkonesh, A.; Namin, M.M.; Buccino, M. Bed compaction effect on dam break flow over erodible bed; experimental and numerical modeling. *J. Hydrol.* **2020**, *594*, 125645. [CrossRef]

59. Di Cristo, C.; Iervolino, M.; Moramarco, T.; Vacca, A. Applicability of Diffusive model for mud-flows: An unsteady analysis. *J. Hydrol.* **2021**, *600*, 126512. [CrossRef]

60. Sarghini, F.; De Vivo, A. Analysis of preliminary design requirements of a heavy lift Multirotor drone for agricultural use. *Chem. Eng. Trans.* **2017**, *58*, 625–630. [CrossRef]

61. Modarelli, G.C.; Arena, C.; Pesce, G.; Dell'Aversana, E.; Fusco, G.M.; Carillo, P.; De Pascale, S.; Paradiso, R. The role of light quality of photoperiodic lighting on photosynthesis, flowering and metabolic profiling in *Ranunculus asiaticus* L. *Physiol. Plant.* **2020**, *170*, 187–201. [CrossRef] [PubMed]

62. Cristofano, F.; El-Nakhel, C.; Rouphael, Y. Biostimulant Substances for Sustainable Agriculture: Origin, Operating Mechanisms and Effects on Cucurbits, Leafy Greens, and Nightshade Vegetables Species. *Biomolecules* **2021**, *11*, 1103. [CrossRef] [PubMed]

63. Crimaldi, M.; Lama, G.F.C. Impacts of riparian plants biomass assessed by UAV-acquired multispectral images on the hydrodynamics of vegetated streams. In Proceedings of the 29th European Biomass Conference and Exhibition, online, 26–29 April 2021; pp. 1157–1161. [CrossRef]

64. Aliberti, A.; Olivieri, F.; Graci, S.; Rigano, M.M.; Barone, A.; Ruggieri, V. Genomic Dissection of a Wild Region in a Superior Solanum pennellii Introgression Sub-Line with High Ascorbic Acid Accumulation in Tomato Fruit. *Genes* **2020**, *11*, 847. [CrossRef]

65. Lama, G.F.C.; Crimaldi, M. Assessing the role of Gap Fraction on the Leaf Area Index (LAI) estimations of riparian vegetation based on Fisheye lenses. In Proceedings of the 29th European Biomass Conference and Exhibition, online, 26–29 April 2021; pp. 1172–1176. [CrossRef]

66. Modarelli, G.C.; Rouphael, Y.; De Pascale, S.; Öztekin, G.B.; Tüzel, Y.; Orsini, F.; Gianquinto, G. Appraisal of Salt Tolerance under Greenhouse Conditions of a *Cucurbitaceae* Genetic Repository of Potential Rootstocks and Scions. *Agronomy* **2020**, *10*, 967. [CrossRef]

67. Olivieri, F.; Calafiore, R.; Francesca, S.; Schettini, C.; Chiaiese, P.; Rigano, M.M.; Barone, A. High-Throughput Genotyping of Resilient Tomato Landraces to Detect Candidate Genes Involved in the Response to High Temperatures. *Genes* **2020**, *11*, 626. [CrossRef] [PubMed]

68. Lama, G.F.C.; Errico, A.; Francalanci, S.; Solari, L.; Chirico, G.B.; Preti, F. Hydraulic Modeling of Field Experiments in a Drainage Channel Under Different Riparian Vegetation Scenarios. In *Innovative Biosystems Engineering for Sustainable Agriculture, Forestry and Food Production*; Coppola, A., Di Renzo, G., Altieri, G., D'Antonio, P., Eds.; Springer: Cham, Switzerland, 2020; pp. 69–77. [CrossRef]

69. Capolupo, A.; Kooistra, L.; Berendonk, C.; Boccia, L.; Suomalainen, J. Estimating Plant Traits of Grasslands from UAV-Acquired Hyperspectral Images: A Comparison of Statistical Approaches. *ISPRS Int. J. Geo-Inf.* **2015**, *4*, 2792–2820. [CrossRef]

70. Fecarotta, O.; Martino, R.; Morani, M.C. Wastewater Pump Control under Mechanical Wear. *Water* **2019**, *11*, 1210. [CrossRef]

71. Forzieri, G.; Guarnieri, L.; Vivoni, E.R.; Castelli, F.; Preti, F. Spectral-ALS data fusion for different roughness parameterizations of forested floodplains. *River Res. Applic.* **2011**, *27*, 826–840. [CrossRef]

72. Piemontese, L.; Castelli, G.; Fetzer, I.; Barron, J.; Liniger, H.; Harari, N.; Bresci, E.; Jaramillo, F. Estimating the global potential of water harvesting from successful case studies. *Glob. Environ. Chang.* **2020**, *63*, 10212. [CrossRef]

73. Liu, D.; Valyrakis, M.; Williams, R. Flow Hydrodynamics across Open Channel Flows with Riparian Zones: Implications for Riverbank Stability. *Water* **2017**, *9*, 720. [CrossRef]

74. Padulano, R.; Rianna, G.; Santini, M. Datasets and approaches for the estimation of rainfall erosivity over Italy: A comprehensive comparison study and a new method. *J. Hydrol. Reg. Stud.* **2021**, *34*, 100788. [CrossRef]

75. Nuzzo, A.; Buurman, P.; Cozzolino, V.; Spaccini, R.; Picoolo, A. Infrared spectra of soil organic matter under a primary vegetation sequence. *Chem. Biol. Technol. Agric.* **2020**, *7*, 6. [CrossRef]

76. Qiu, J.; Cao, B.; Park, E.; Yang, X.; Zhang, W.; Tarolli, P. Flood Monitoring in Rural Areas of the Pearl River Basin (China) Using Sentinel-1 SAR. *Remote Sens.* **2021**, *13*, 1384. [CrossRef]